Cobalt Oxide (Co_4O_6)

Timothy Mayowa Akintayo

Gdansk University of Technology, Gdansk, Poland

Abstract

This study investigates the effect of spin multiplicity on the stability of cobalt oxide clusters Co_4O_6 and $Co_2O_3^{-1}$ using quantum mechanical calculations. The Unrestricted Hartree-Fock (UHF) method was employed in the GAMESS computational package to optimize molecular geometries and analyze electronic structure across multiple spin states over the Gdansk University of Technology's supercomputer. Spin 8 was identified as the most stable configuration for Co_4O_6, while for the anionic $Co_2O_3^{-1}$, spin ($\frac{17}{2}$) exhibited the lowest energy but underwent structural changes, suggesting spin $\frac{19}{2}$ as a more stable alternative. Comparative analysis with colleagues' results confirmed that spin 8 is the most energetically favorable state across different Co_4O_6 configurations. The findings provide insight into spin-dependent stability in transition metal oxides, which is essential for applications in catalysis and battery materials.

1 Introduction

Quantum chemistry offers important tools to understand the electronic and structural properties of materials, especially transition metal oxides. These compounds are often studied for their electronic, catalytic, and magnetic characteristics. With quantum chemical cal-

culations, we gain insight into the electronic structure, bonding, and stability of molecular systems, particularly transition-metal clusters. These calculations are carried out using different quantum mechanical methods, which help predict molecular properties, including geometry, energy levels, and electronic configurations.

In this study, we performed a quantum mechanical simulation of cobalt tetroxide (Co_4O_6) and the anionic $Co_2O_3^{-1}$ using the General Atomic and Molecular Electronic Structure System (GAMESS) package which was run on a supercomputer. The simulation involved optimizing the geometry of the two molecules at different spin states. This helped to explore the spin multiplicity effects on the system's stability. This study examined 11 successive spin states for both (Co_4O_6) and $Co_2O_3^{-1}$. By examining different spin states, we can determine the most stable configuration in line with the initial geometry and its electronic properties. This analysis is beneficial for understanding the behavior of cobalt oxides in real-world applications, such as battery materials and catalysis, where stability and electronic structure play important roles.

2 Methods

2.1 Computational Tools

For this simulation the quantum chemistry package known as General Atomic and Molecular Electronic Structure System (GAMESS), molden software, Chemcraft, and the Gdansk super computer were used.

2.2 Unrestricted Hartree-Fock (UHF)

Using the Unrestricted Hartree-Fock (UHF) method [1], the electronic structure of Co_4O_6 and $Co_2O_3^{-1}$ were studied. The Hartree-Fock equation for each spin component is presented below:

$$F^{\sigma}\psi_i^{\sigma} = \varepsilon_i \psi_i^{\sigma}, \quad \sigma \in \{\alpha, \beta\} \tag{1}$$

where F^{σ} is the Fock operator, ψ_i^{σ} represents the molecular orbitals, α is spin-up and β is spin-down, and ε_i are the orbital energies.

The UHF method treats beta and alpha electrons independently, which allows a better description of systems with unpaired electrons, such as transition metal oxides [1].

2.3 Self-Consistent Field (SCF)

To solve the Hartree-Fock equations iteratively, the Self-Consistent Field (SCF) method was used. The SCF energy convergence criterion is:

$$E_{\text{SCF}}^{(n+1)} - E_{\text{SCF}}^{(n)} < \delta \tag{2}$$

where δ is the convergence threshold (e.g., 10^{-6} Hartree) [4].

2.4 Basis Set and Effective Core Potential (ECP)

The SBKJC basis set used in this simulation expands the wavefunction as follows:

$$\psi_i(\mathbf{r}) = \sum_{\mu} C_{\mu i} \chi_\mu(\mathbf{r}) \tag{3}$$

where $\chi_\mu(\mathbf{r})$ are atomic basis functions and $C_{\mu i}$ are the molecular orbital coefficients.

The effective core potential (ECP) replaces inner core electrons with an analytical function:

$$V_{\text{ECP}}(\mathbf{r}) = \sum_{lm} C_{lm} Y_{lm}(\theta, \phi) r^n e^{-\alpha r} \tag{4}$$

where $Y_{lm}(\theta, \phi)$ are spherical harmonics.

2.5 Rational Function Optimization (RFO)

For the optimization of the geometry, the Rational Function Optimization (RFO) method was used. This is a second-order optimization technique that efficiently finds minima by constructing a rational function approximation of the energy surface. The method updates atomic positions using the inverse Hessian matrix and the energy gradient:

$$\mathbf{x}_{n+1} = \mathbf{x}_n - \mathbf{H}^{-1} \nabla E$$

where $\mathbf{x}$ represents the atomic positions, $\mathbf{H}$ is the Hessian matrix (or its approximation), and ∇E is the energy gradient. The RFO method improves convergence by stabilizing the optimization path, especially near saddle points, making it more reliable than standard gradient descent methods.

2.6 Optimization of the Geometry

After obtaining the electronic structure, the molecular geometry was optimized to find the lowest energy configuration. The key steps in this procedure were:

- **Building the Initial Geometry:** The simulation process commenced with constructing the initial molecular geometry in the Z-matrix format from the Molden software by defining the bond lengths, angles, and dihedrals relative to the reference atom.

- **Force Calculation:** A calculation of the forces in each atom was performed using the total energy gradient. It is represented with the formula below:

$$F_i = -\frac{\partial E}{\partial r_i} \tag{4}$$

- **Optimization:** A second order optimzation technique named Rational Function Optimization (RFO) was used to optimize the geometry.

- **Convergence Criteria:** The optimization was considered complete and valid when the energy change between the optimization steps was less than 10^{-5} Hartree.

3 Results and Discussion

3.1 Initial and Optimized Geometry of Co_4O_6

The optimized molecular structure image of Co_4O_6 for each spin considered 1 to 10 were obtained using the Chemcraft visualization tool and presented below.

Neutral Molecule (Co_4O_6)

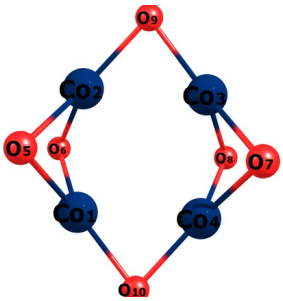

Figure 1: Spin 0 Initial

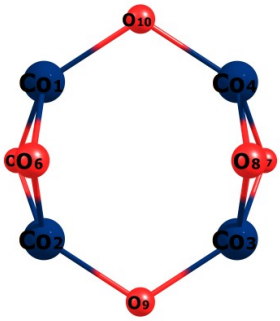

Figure 2: Spin 0 Optimized

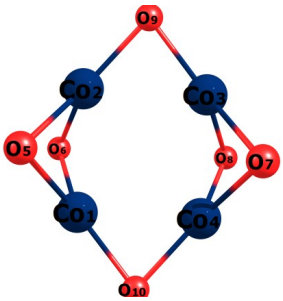

Figure 3: Spin 1 Initial

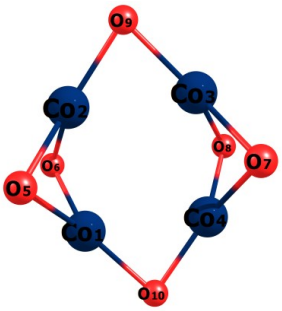

Figure 4: Spin 1 Optimized

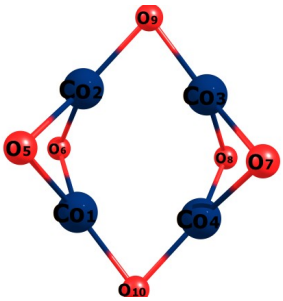

Figure 5: Spin 2 Initial

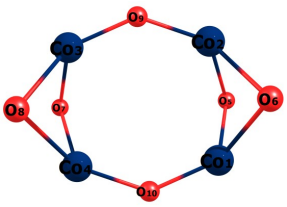

Figure 6: Spin 2 Optimized

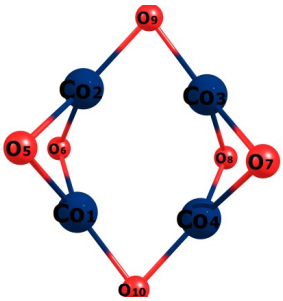

Figure 7: Spin 3 Initial

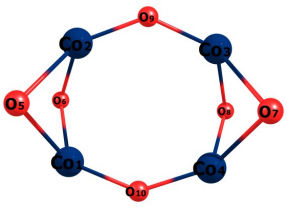

Figure 8: Spin 3 Optimized

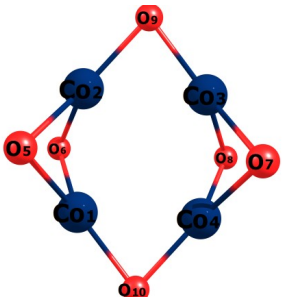

Figure 9: Spin 4 Initial

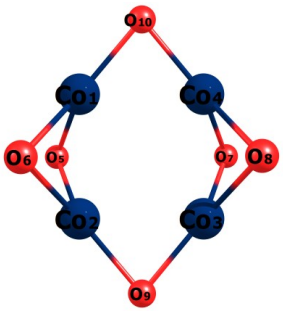

Figure 10: Spin 4 Optimized

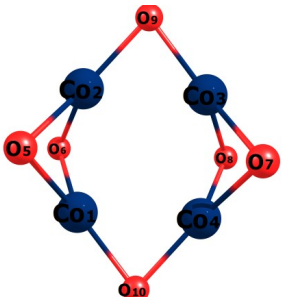

Figure 11: Spin 5 Initial

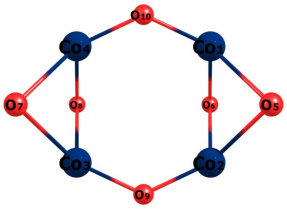

Figure 12: Spin 5 Optimized

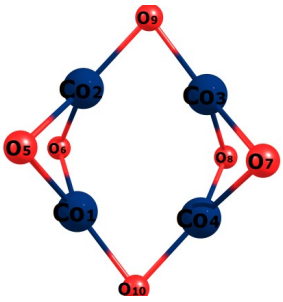

Figure 13: Spin 6 Initial

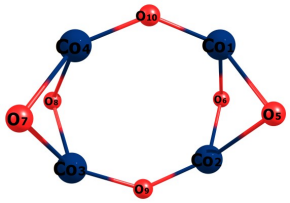

Figure 14: Spin 6 Optimized

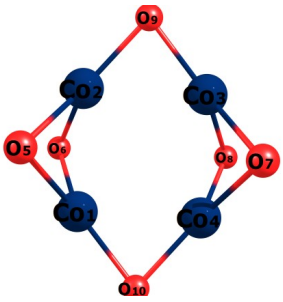

Figure 15: Spin 7 Initial

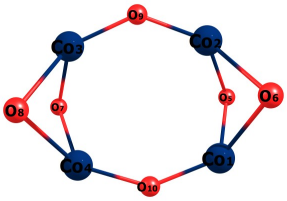

Figure 16: Spin 7 Optimized

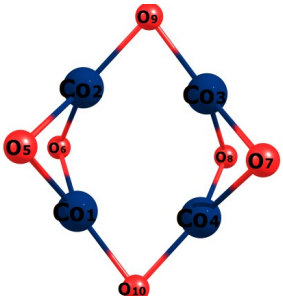

Figure 17: Spin 8 Initial

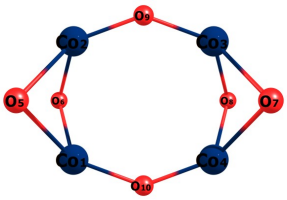

Figure 18: Spin 8 Optimized

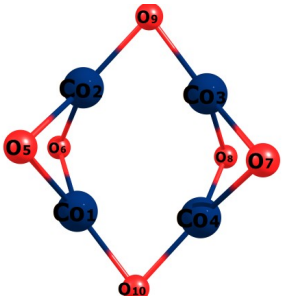

Figure 19: Spin 9 Initial

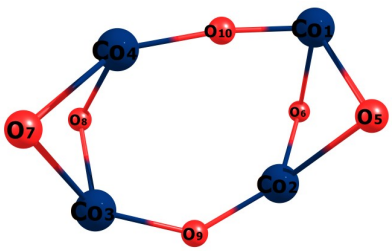

Figure 20: Spin 9 Optimized

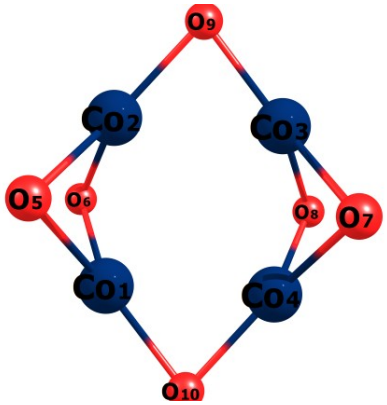

Figure 21: Spin 10 Initial

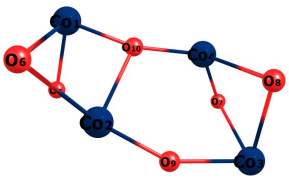

Figure 22: Spin 10 Optimized

3.2 Initial and Optimized Geometry $Co_2O_3^{-1}$

The optimized molecular structure of $Co_2O_3^{-1}$ for each spin considered $\frac{0}{2}$ to $\frac{21}{2}$ obtained using the Chemcraft software and presented below:

Anionic Molecule

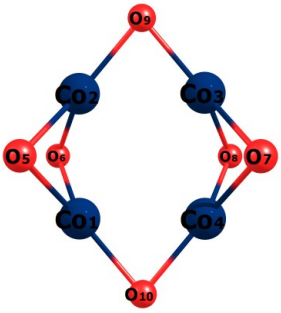

Figure 23: Spin $\frac{0}{2}$ Initial

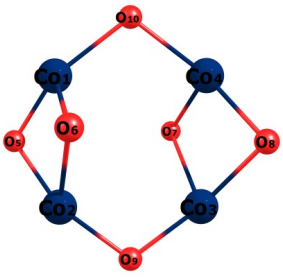

Figure 24: Spin $\frac{0}{2}$ Optimized

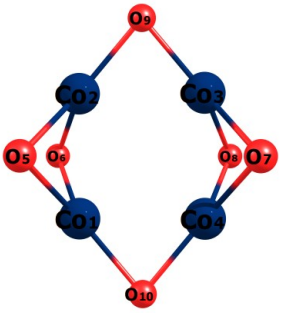

Figure 25: Spin $\frac{3}{2}$ Initial

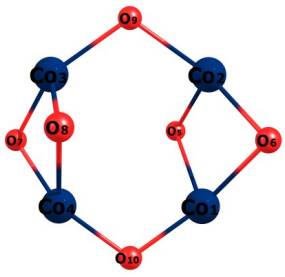

Figure 26: Spin $\frac{3}{2}$ Optimized

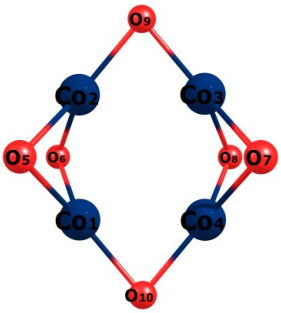

Figure 27: Spin $\frac{5}{2}$ Initial

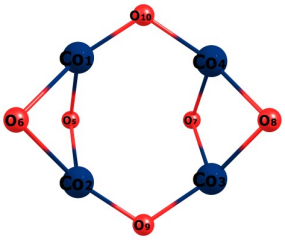

Figure 28: Spin $\frac{5}{2}$ Optimized

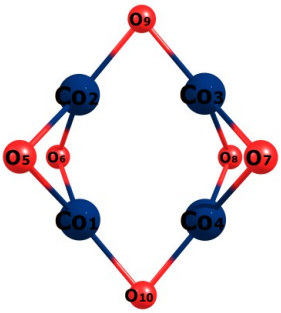

Figure 29: Spin $\frac{7}{2}$ Initial

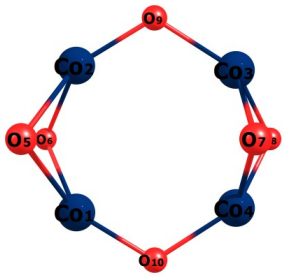

Figure 30: Spin $\frac{7}{2}$ Optimized

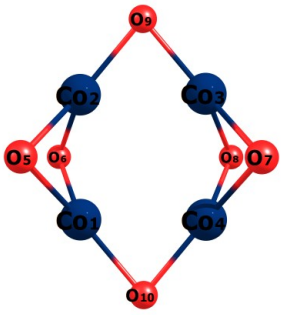

Figure 31: Spin $\frac{9}{2}$ Initial

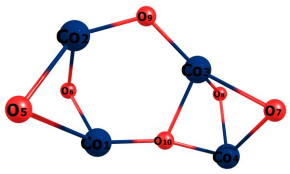

Figure 32: Spin $\frac{9}{2}$ Optimized

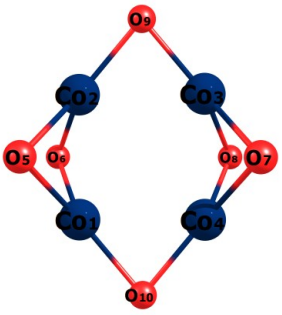

Figure 33: Spin $\frac{11}{2}$ Initial

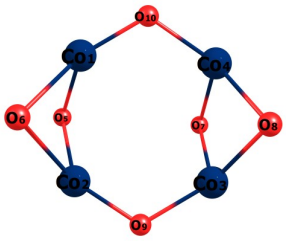

Figure 34: Spin $\frac{11}{2}$ Optimized

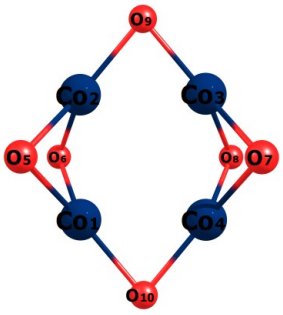

Figure 35: Spin $\frac{13}{2}$ Initial

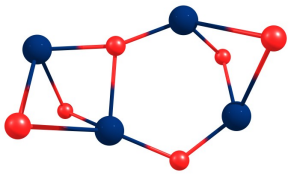

Figure 36: Spin $\frac{13}{2}$ Optimized

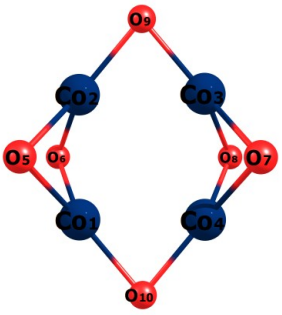

Figure 37: Spin $\frac{15}{2}$ Initial

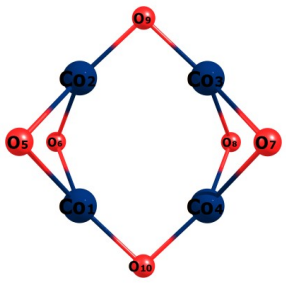

Figure 38: Spin $\frac{15}{2}$ Optimized

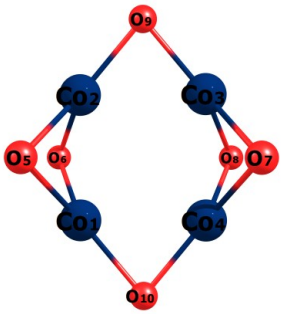

Figure 39: Spin $\frac{17}{2}$Initial

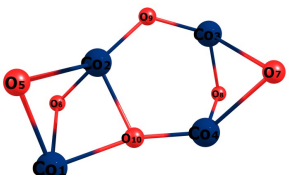

Figure 40: Spin $\frac{17}{2}$ Optimized

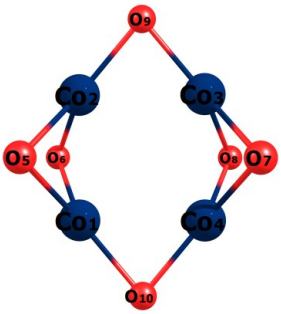

Figure 41: Spin $\frac{19}{2}$ Initial

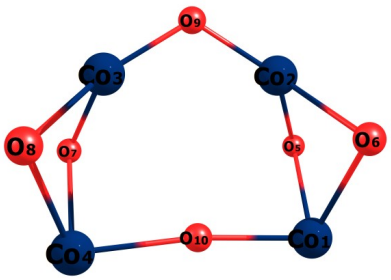

Figure 42: Spin $\frac{19}{2}$ Optimized

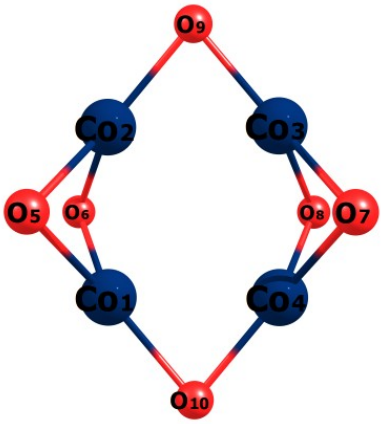

Figure 43: Spin $\frac{21}{2}$ Initial

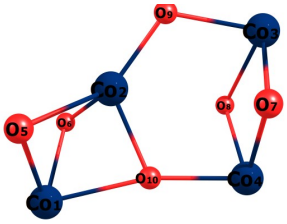

Figure 44: Spin $\frac{21}{2}$ Optimized

3.3 Interpretation of Co_4O_6

From the presented images of the initial and final geometry, it is observed that the initial and optimized structure for spin 1 to 8 remains unchanged, indicating that the electronic configuration remains energetically favorable without major distortions across these spin states. However, in spin 9 and 10, there is noticeable geometric changes after optimization, indicating that beyond spin 8, the electronic structures reconfigures to a new minimum energy geometry. This is perhaps due to spin-state crossover, where electron redistribution between the cobalt d- orbitals brings about a change in the metal-ligand interactions. In addition, the Jahn-Teller effect could also be cause of this. This effect often arises when degenerate electronic states at higher spins trigger asymmetry in the final geometry.

3.4 Interpretation of $Co_2O_3^{-1}$

The anionic molecule had an earlier instability occurring at spin $\frac{9}{2}$, spin $\frac{13}{2}$, spin $\frac{17}{2}$ and spin $\frac{21}{2}$. Unlike the neutral, the anionic exhibited an earlier distortion at spin $\frac{9}{2}$, meaning that the extra electron leads to pertubation which affects the electronic balance even at lower spin threshold. At these 4 spin states, the initial and optimized geometry structures differ significantly. We can surmise that the extra charge led to a more mixed spin state, thereby increasing electronic competition and resulting in instability at those spin values whose geometries differ.

3.5 Spin State and Energy Analysis

The total energy of a system depends on the spin multiplicity M, given by:

$$M = 2S + 1 \tag{5}$$

where S is the total spin quantum number. The energy differences for different spin states are computed as:

$$\Delta E = E_S - E_{\text{min}} \tag{6}$$

where E_{min} is the lowest computed energy [6]. The relative energy is calculated as:

$$E_{\text{rel}} = (E_{\text{ith spin}} - E_{S=8}) \times 627.509 \text{ kcal/mol} \tag{7}$$

where:

- $E_{\text{ith spin}}$ is the total energy of the system for a particular spin state. The energy is negative because these are bound states (i.e., the system is stable).
- $E_{S=8}$ is the energy of the system for the $S = 8$ eight state.
- The conversion factor is the conversion factor from Hartree to kcal/mol, which has a value of 627.509.
- Relative energy (kcal/mol): This refers to the difference in energy between a given spin state and a reference spin state, typically the lowest energy state (often $S = 8$, in this case) multiplied by the conversion factor.

3.6 Electronic Structure and Spin States

The calculated energies for each spin from 1 to 10 and $\frac{1}{2}$ to $\frac{21}{2}$ are presented in this section.

3.7 Table of Energy vs Spin and Multiplicity For the Co_4O_6

Mult.	Spin	Energy	Rel. Energy
1	0	-670.9638155229	191.5888157
3	1	-671.0038022063	166.4968119
5	2	-671.1287031139	88.1203683642
7	3	-671.0623134388	129.7804869965
9	4	-671.0026744103	167.2045141315
11	5	-671.0026744285	167.2045027109
13	6	-671.1338501088	84.8905827415
15	7	-671.2015197506	42.4272734852
17	8	-671.2691319657	0.0000000000
19	9	-671.1799139651	55.9850983385
21	10	-671.1516579305	73.7160143543

From the table of total and relative energy for the neutral molecule presented above, It can be seen that spin 8 yielded the lowest total energy, indicating that it is the most stable electronic configuration. Spin 9 and 10 exhibited slightly different geometry after optimization as discussed in the initial and optimized geometry section of this study. A plot of the relative energy and spin which will help to further see how this difference in geometry of the 9th and 10th spin affects the overall trend of the relative energy is presented in the next section

3.8 Plot of Spin vs Relative Energy Co_4O_6

To understand the effect of the spin multiplicity on the stability of both molecules, a plot of the relative energy against each spin state is done for Co_4O_6.

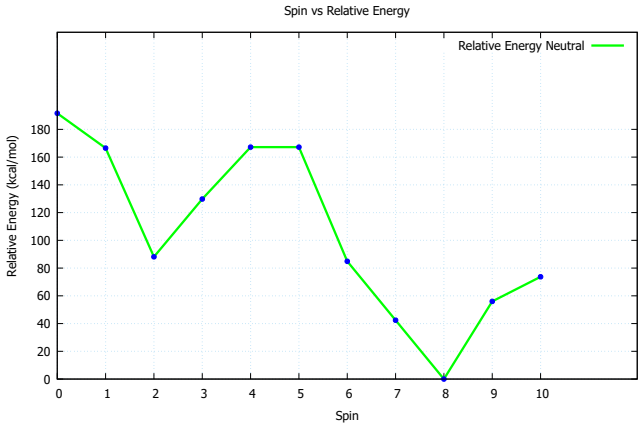

Figure 45. Relative Energy vs Spin (Neutral)

The presented plot shows a non-monotonic trend. From spin 0 to spin 2, the relative energy decreases, indicating increasing stability. However, at spin 3, the trend reverses as the relative energy slightly increases up to spin 4. Between spin 4 and 5, the relative energy remained nearly constant suggesting a temporary equilibrium states which was short-lived. From spin 5 to spin 8, the relative energy continues to decrease, reaching its minimum at spin 8, which corresponds to the most stable electronic configuration. At spin 9 and spin 10, the energy begins to increase again, indicating that higher spin states are less stable than spin 8. The reversal in trend beyond spin 8 correlates with the geometric distortions observed in the optimized structures for spin 9 and 10 in the geometric discussion section of the study. The structural changes is likely after the electron redistribution, reducing the energetic favorability of these higher spin states.

3.9 Table of Energy vs Spin and Multiplicity For the $Co_2O_3^{-1}$

Mult.	Spin	Energy	Rel. Energy
2	$\frac{1}{2}$	-671.0421919	169.3555914
4	$\frac{3}{2}$	-671.0396701	170.938056
6	$\frac{5}{2}$	-671.0520798	163.1508601
8	$\frac{7}{2}$	-671.0513806	163.5896314
10	$\frac{9}{2}$	-671.0324694	175.4566042
12	$\frac{11}{2}$	-671.1812358	82.10432594
14	$\frac{13}{2}$	-671.1687322	89.95043229
16	$\frac{15}{2}$	-671.2774474	21.73066453
18	$\frac{17}{2}$	-671.3120775	0.0000000000
20	$\frac{19}{2}$	-671.2832357	18.09847339
22	$\frac{21}{2}$	-671.2555414	35.47690028

From the presented table, it can be seen that spin ($\frac{17}{2}$) had the lowest total energy which should ideally make it the most stable configuration. However, because the molecule exhib-

ited a significantly different structure after optimization at this spin state, we cannot completely regard it as the most stable configuration. Hence, the stable configuration is spin $\frac{19}{2}$.

3.10 Plot of Spin against Relative Energy $Co_2O_3^{-1}$.

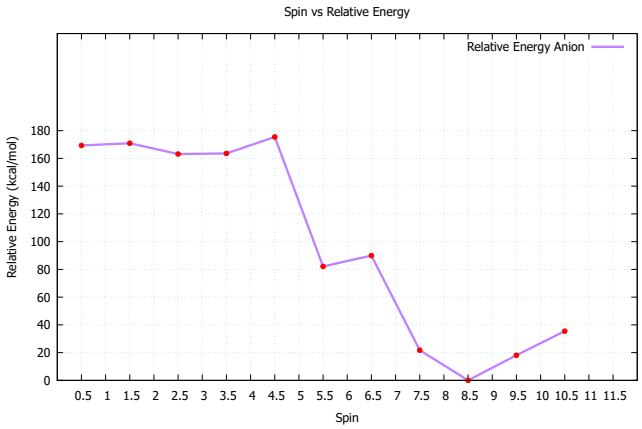

Figure 46. Relative Energy vs Spin (Anionic)

From the presented plot, it can be observed that the relative energy for the anionic molecule exhibits a more fluctuating pattern compared to the neutral molecule. From spin $\frac{1}{2}$ to spin $\frac{5}{2}$, the relative energy decreases but not as smoothly as in the neutral molecule. At spin $\frac{7}{2}$ and spin $\frac{9}{2}$, the relative energy increases again showing early instability in the anion. It is important to state that at $\frac{9}{2}$, a structural change was observed as discussed earlier in the geometry section. Here the energy increased instead of decreasing, indicating that the system undergoes a geometric rearrangement. Between spin $\frac{9}{2}$, to $\frac{13}{2}$, the energy stabilizes but another structural changed occurred at $\frac{13}{2}$, causing further instability. From this spin to spin $\frac{17}{2}$, the energy continued to decrease. While spin 8.5 had the lowest relative energy, we cannot consider it the stable configuration because the optimized structure in this state, differed from the initial. Between spin $\frac{17}{2}$ and spin $\frac{21}{2}$, the trend reverses again and the energy increases again due to structural reconfiguration.

3.11 Comparative Plot of Co_4O_6 and $Co_2O_3^{-1}$

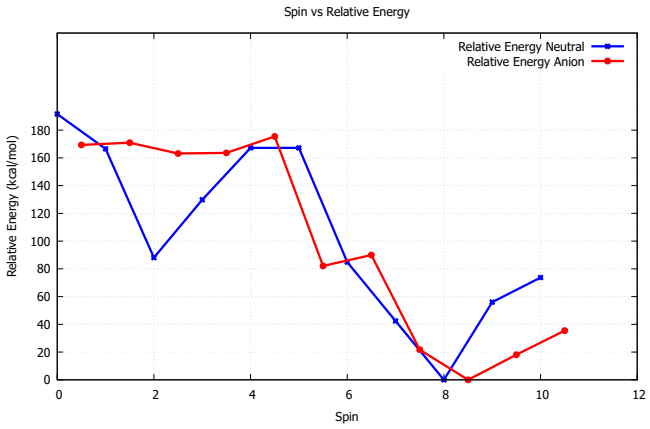

Figure 47. Relative Energy and Anionic Plot

From the above presented plot, it can be seen that both the neutral and anionic system exhibit a general decrease in relative energy. However, the anionic system exhibits larger energy fluctuations, even in lower spin states pos-

sibly due to charge-induced instability. This behavior shows that the neutral system is more stable across multiple spin states and that the anionic molecule experiences structural distortions at earlier spin states, which is a signal of increased sensitivity to spin state variations. The structural changes observed at $\frac{9}{2}$, $\frac{13}{2}$, $\frac{17}{2}$, and $\frac{21}{2}$ is an indication that the extra electron in the anionic system introduces instability at these spin states. The instability is possibly due to electron repulsions disrupting orbital hybridization, leading to a geometric shift that affects the bonding patterns.

3.12 Comparison of Colleague's Co_4O_6 Results

Configuration	Spin	Energy
D1	7	-671.20997
D2	8	-671.20743
D4	6	-671.2253
D5	5	-671.1519
D7	8	-671.2691
D8	8	-671.3010
D10	8	-671.2204
D15	8	-671.2691
D16	6	-671.1736

Table 1: Energy configurations from colleagues for Co_4O_6.

The above presented table is the total energy value of the neutral system from my colleagues. This table shows that D8 is the lowest energy configuration with -671.3010 Ha. This indicates that spin 8 is the most stable spatial configuration among all the studied cases of the neutral system of Co_4O_6. It can be seen that most stable structures occur at spin 8, which corresponds with the trend observed in the neutral Co_4O_6 of this study. The spin 6 and spin 7 configurations (D4, D1, D16) have slightly higher energy, meaning they are less stable than spin 8. The highest energy structure is (D5, spin 5, -671.1519 Ha), indicating that they are the least stable among the configurations.

4 Conclusion

This study utilized GAMES to perform a geometry optimization of Co_4O_6 and $Co_2O_3^{-1}$ using the Unrestricted Hartree-Fock (UHF) method. This optimization procedure showcased the importance of spin multiplicity in determining molecular stability by analyzing stability across 11 different spin states. In the neutral molecule, spin 8 was the stable configuration while in the anionic spin $\frac{17}{2}$ was the stable configuration. However, we cannot completely agree that it is the most stable configuration because there was structural change after optimization in this spin state based on the geometric presentation in the study. This brings us to the need to regard spin $\frac{19}{2}$ as the most stable because it is the second minimum energy state

based on the total energy of the Hartree. A comparative analysis of the stable configuration of this system with that of my colleagues also showed that overall spin 8 had the most stable configuration across different Co_4O_6 variants considered.

5 References

1. Jensen, F. (2017). *Introduction to Computational Chemistry*. Wiley. Available at: https://www.wiley.com

2. Szabo, A., & Ostlund, N. S. (1996). *Modern Quantum Chemistry: Introduction to Advanced Electronic Structure Theory*. Dover. Available at: https://www.doverpublications.com

3. Stevens, W. J., Basch, H., & Krauss, M. (1984). Compact effective potentials and efficient shared-exponent basis sets for the first- and second-row atoms. *The Journal of Chemical Physics, 81*(12), 6026–6033. Available at: https://doi.org/10.1063/1.447604

4. Roothaan, C. C. J. (1951). New developments in molecular orbital theory. *Reviews of Modern Physics, 23*(2), 69-89. Available at: https://doi.org/10.1103/RevModPhys.23.69

5. Pulay, P. (1980). Convergence acceleration of iterative sequences. The case of SCF iteration. *Chemical Physics Letters, 73*(2), 393–398. Available at: https://doi.org/10.1016/0009-2614(80)80396-4

6. Szabo, A. (1989). Spin and stability in transition metal oxides. *Journal of Chemical Theory and Computation, 5*(3), 567–575. Available at: https://doi.org/10.1021/ct900004k